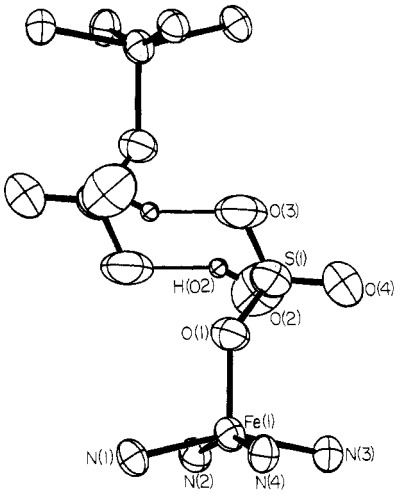

Figure 4. ORTEP diagram illustrating the hydrogen-bond arrangement between an inversion-related pair of [Fe(TPP)(OSO_3H)] molecules.

of perchlorate metalloporphyrin derivatives,[28] another group of oxyanion-ligated species, are all close to 0°, an orientation that minimizes the nonbonded interactions between porphinato core atoms and the oxygens. In [Fe(TPP)(OSO_3H)], these interactions are minimized by an increased value for the Fe–O–S bond angle (135.0°), an increase of 5–10° over the analogous angle in the various perchlorates.

The unidentate HSO_4^- ion in both molecules has the same interesting pattern in its S–O distances. Each S–O distance in the ion appears to be different from the others. As might be expected, the longest S–O distance in each ion involves the oxygen atom bonded to the hydrogen atom of the HSO_4^- ion; the next longest involves the oxygen atom coordinated to the iron(III) porphyrinate. The oxygen atom that is the hydrogen-bond acceptor is next longest, while the shortest distance involves the oxygen atom that is simply bonding to sulfur. For the reader's convenience, the S–O distances of Table III are organized in the order of the above interactions; the strong similarity in values between the two molecules is evident.

The hydrogen bonding between pairs of molecules in [Fe(TPP)(OSO_3H)] and the resultant effect that leads to the various types of S–O bonds (Table III) suggest that there should be equivalent effects on the HSO_4^- vibrational spectra. It is thus reasonable to suggest that the identity of the SO_2-I species is a non-hydrogen-bonded solid-state form of [Fe(TPP)(OSO_3H)]. It further seems plausible that the observed hydrogen-bond interactions serve to stabilize the anion in its bisulfate form and retard the conversion of [Fe(TPP)(OSO_3H)] to $[Fe(TPP)]_2SO_4$.

Acknowledgment. We thank the National Institutes of Health (Grant GM-38401-16) for support.

Supplementary Material Available: Figure S1, showing an ORTEP diagram of molecule 2, and Tables SI–SV, listing complete crystal data and intensity collection parameters, anisotropic temperature factors for all atoms, fixed hydrogen atom coordinates, and complete tables of bond distances and angles in the two molecules (13 pages); a table of observed and calculated structure factors (×10) (20 pages). Ordering information is given on any current masthead page.

(28) (a) Spaulding, L. D.; Eller, P. G.; Bertrand, J. A.; Felton, R. H. *J. Am. Soc.* **1974**, *96*, 982–987. (b) Song, H.; Rath, N.; Reed, C. A.; Scheidt, W. R. To be submitted for publication. (c) Barkigia, K. M.; Spaulding, L. D.; Fajer, J. *Inorg. Chem.* **1983**, *22*, 349–351. (d) Reed, C. A.; Mashiko, T.; Bentley, S. P.; Kastner, M. E.; Scheidt, W. R.; Spartalian, K.; Lang, G. *J. Am. Chem. Soc.* **1979**, *101*, 2948–2958. (e) Masuda, H.; Taga, T.; Osaki, K.; Sugimoto, H.; Yoshida, Z.-I.; Ogoshi, H. *Inorg. Chem.* **1980**, *19*, 950–955. (f) Gans, P.; Buisson, G.; Duee, E.; Marchon, J.-C.; Erler, B. S.; Scholz, W. F.; Reed, C. A. *J. Am. Chem. Soc.* **1986**, *108*, 1223–1234.

Contribution from the NMR Section, Department of Radiology, Massachusetts General Hospital and Harvard Medical School, Boston, Massachusetts 02114

Solution Structure and Dynamics of Lanthanide(III) Complexes of Diethylenetriaminepentaacetate: A Two-Dimensional NMR Analysis

Bruce G. Jenkins and Randall B. Lauffer*

Received June 27, 1988

The solution structure and dynamics of lanthanide(III) complexes of diethylenetriaminepentaacetate (DTPA) have been investigated by ^1H NMR. Two-dimensional (2D) exchange spectroscopy (EXSY) enables the determination of solution dynamics. At low temperatures (0–25 °C) the complexes $Pr(DTPA)^{2-}$, $Eu(DTPA)^{2-}$, and $Yb(DTPA)^{2-}$ are in slow exchange on the NMR time scale, and all 18 proton chemical shifts are resolved. Raising the temperature causes the number of resonances to decrease from 18 to 9, consistent with exchange between two enantiomers. The rates of exchange of the complexes follow the order Pr(III) < Eu(III) < Yb(III). Utilization of 2D correlation spectroscopy (COSY) along with EXSY data as constraints enables assignments of the chemical shifts via calculations of the dipolar shifts. These calculations afford many reasonable solutions with low *R* factors, and only through the use of the 2D COSY and EXSY data can certain solutions be rejected. These calculations also confirm that the previously published crystal structure of $Nd(DTPA)^{2-}$ can quite satisfactorily explain the solution structure. In addition, these data indicate that the central acetate moiety is coordinated to the metal in solution.

Introduction

The solution structure and dynamics of multidentate lanthanide(III) complexes are not well understood. These complexes generally have coordination numbers of 8–10 with greatly varying coordination polyhedra.[1,2] Questions that arise include the following: (i) Are the solution structures the same as that in the solid state? (ii) Can the total coordination number vary as a function of temperature or across the lanthanide series? (iii) What factors control the intramolecular dynamics?

The importance of these issues has been enhanced by the recent development of gadolinium(III) complexes as diagnostic pharmaceuticals for clinical ^1H NMR imaging.[3] These agents are injected intraveneously to alter the water proton relaxation times of tissues and improve image contrast and information content. The prototype agent, aquogadolinium(III) diethylenetriaminepentaacetate [$Gd(DTPA)(H_2O)^{2-}$], has undergone extensive clinical trials[4] and is now approved for human use in the U.S. It

(1) Williams, R. J. P. *Struct. Bonding* **1982**, *50*, 79.
(2) Sinha, S. P. *Struct. Bonding* **1976**, *45*, 69.
(3) Lauffer, R. B. *Chem. Rev.* **1987**, *87*, 901.

0020-1669/88/1327-4730$01.50/0

is important to fully characterize solution chemistry of such chelates both to understand the in vivo behavior and to design improved agents. Critical features include the coordination of water to the metal center and the kinetic stability of the complexes in aqueous solution.[3]

While transition-metal chelates of DTPA have been studied in solution,[5,6] extensive studies of the lanthanide(III)–DTPA chelates have not emerged. The crystal structures of the neodymium(III) and gadolinium(III) complexes reveal full octadentate chelation by DTPA and a single coordinated water.[7,8] However, ^{1}H NMR studies of the lanthanum(III) and lutetium(III) derivatives have been interpreted as indicating that the central acetate is not coordinated in solution.[9] This question is of importance with regard to the water proton relaxation efficiency of NMR contrast agents since an extra site for coordination of water to a paramagnetic metal has the potential of increasing the relaxivity considerably (cf. ref 3).

In this study we utilize two-dimensional (2D) NMR techniques on both diamagnetic and paramagnetic Ln(DTPA)$^{2-}$ complexes to address the structural and dynamic aspects of these complexes in solution. These and our previous data[10] indicate that in solution Ln(DTPA)$^{2-}$ chelates exist in two symmetric forms that undergo dynamic chemical exchange. The rates of this exchange are comparable to those seen for the polyamino polycarboxylate ligands in Ln(DOTA)$^-$ and Ln(TETA)$^-$;[11,12] thus, Ln(DTPA)$^{2-}$ is relatively "rigid". In addition, our results provide unequivocal evidence for coordination of the central acetate.

Experimental Section

DTPA Samples. Stoichiometric amounts of DTPA (Aldrich Chemical Co., 97% pure) and $LnCl_3 \cdot 6H_2O$ (Aldrich 99.999% or Alfa 99.9%) were added to D_2O and the mixture stirred at 80 °C. Small amounts of concentrated NaOD were titrated into the solution until the pH was between 7 and 8 (uncorrected for deuterium isotope effect). The solutions were then filtered into NMR tubes to remove any residual solids. NMR spectra were obtained to ascertain the proper stoichiometry of the complexes. In some cases a small excess (<1:10) of free DTPA was noted; however, no exchange with the Ln(DTPA)$^{2-}$ complexes was noted under any conditions studied. NMR spectra of La(DTPA)$^{2-}$ were identical with those reported previously.[9]

Partial deuteriation of the acetates was achieved by stirring a solution of free DTPA in D_2O at pH 11 (NaOD) at 90–95 °C. After 25 h under these conditions deuteriation of the terminal acetates was 54–57% and that of the central acetate was 44–45%. These ratios were determined by integration of the ^{1}H NMR spectra of the free ligands at pH 3. Deuteriation of the acetates was utilized to confirm assignments of proton resonances as belonging to either acetates or ethylenes.

NMR Measurements and Calculations. NMR measurements were made at either 500, 300, or 250 MHz. Those at 500 MHz were collected at the Francis Bitter National Magnet Laboratory at the Massachusetts Institute of Technology on a home-built spectrometer. All other spectra were collected on either a Bruker AM300 or AM250 instrument at the Harvard University Chemistry Department. Chemical exchange was probed by using the standard 90°–t_1–90°–τ_m–90° (NOESY) 2D pulse sequence[13] where t_1 is the evolution time during which spins develop frequency labeling and τ_m is the mixing time during which spins exchange magnetizations. Phase cycling was utilized to generate pure absorption mode spectra.[14] Since exchange effects are being monitored rather than nuclear Overhauser effects, we shall refer to these as EXSY spectra rather than NOESY spectra. Two-dimensional correlation spectra were acquired by using a phase-sensitive COSY.[15] Chemical shifts are reported with respect to TSP.

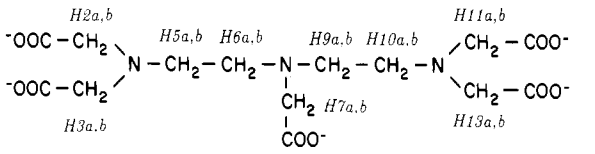

Figure 1. Schematic of the free ligand DTPA with proton labels corresponding to those in ref 7 and assigned to NMR chemical shifts for the Pr(III) and Yb(III) complexes in Tables II and III.

Some of the exchange rates reported were calculated from 2D EXSY spectra in the initial rate regime (i.e. where $\tau_m \leq 1/k_{ex}$) by use of the following method. If we assume a simple two-site interchange between symmetry-related species (in which case k_{ex}(forward) = k_{ex}(backward)) where the protons have similar T_1's and intensities, then diagonal and cross-peak intensities are

$$I(\text{diag}) = \tfrac{1}{2}[1 + \exp(-2k_{ex}\tau_m)][\exp(-\tau_m/T_1)]I_0$$

$$I(\text{cross}) = \tfrac{1}{2}[1 - \exp(-2k_{ex}\tau_m)][\exp(-\tau_m/T_1)]I_0 \quad (1)$$

If $\tau_m \leq 1/k_{ex}$ (such that cross peaks have smaller intensities than diagonal peaks) then the above expressions can be rearranged to

$$k_{ex} = \tfrac{1}{2}\tau_m \ln [(1 + I_c/I_d)/(1 - I_c/I_d)] \quad (2)$$

Note that I_c and I_d represent volumes. Since the ratio of volumes is all that is necessary, we can determine the ratio of volumes by comparing the frusta of the approximate diagonal- and cross-peak cones:

$$\text{volume frustrum (cross)} = \tfrac{1}{3}\pi h_c(R_c^2 + r_c^2 + R_c r_c)$$

$$\text{volume frustrum (diag)} = \tfrac{1}{3}\pi h_d(R_d^2 + r_d^2 + R_d r_d) \quad (3)$$

We then compare the cross- and diagonal-peak radii at two different contour levels (i.e. R and r are the larger and smaller radii). In this case the heights, h, will be equal and hence

$$\frac{I_c}{I_d} = \frac{R_c^2 + r_c^2 + R_c r_c}{R_d^2 + r_d^2 + R_d r_d} \quad (4)$$

This method will work if we assume that apodization produces nearly circular line shapes and if contour levels are chosen intermediate between the base and vertex of the peaks. In addition, the only peaks chosen were those that were of equal intensity. The mixing times used in these k_{ex} determinations varied between 0.5 and 1.5 ms.

Other exchange rates were determined by coalescence temperatures from data obtained at both 500 and 300 MHz after correction for the temperature dependencies of the chemical shifts. Since the EXSY spectra allow us to assign *all* exchange partners, coalescence temperatures can be recorded over a wide temperature range, allowing for more accurate exchange activation parameters than are normally associated with this technique.[16] This assumes, of course, that one can accurately correct for the temperature dependence of the paramagnetic shifts. The temperatures covered by this technique ranged from ≈0 to 85 °C.

Chemical shift calculations were performed by assuming both axial and nonaxial symmetry using the dipolar equations for the isotropic shifts (i.e. δ(iso) = δ(LnDTPA) − δ(LaDTPA))

$$\delta = D_1\left\langle \frac{3\cos^2\theta - 1}{r^3} \right\rangle \quad (5)$$

$$\delta = D_1\left\langle \frac{3\cos^2\theta - 1}{r^3} \right\rangle + D_2\left\langle \frac{\sin^2\theta \cos 2\phi}{r^3} \right\rangle \quad (6)$$

where r, θ, and ϕ are the spherical polar coordinates of the proton relative to the magnetic susceptibility axes and D_1 and D_2 are the dipolar constants that are related to the anisotropy of the magnetic susceptibility of the paramagnetic complex. The geometric factors above were determined from proton coordinates reported in the crystal structure of NdDTPA.[7] Fits to the observed chemical shifts were performed by using a computer program kindly provided by Dr. A. Dean Sherry,[17] as well as a program

(4) Runge, V. M., Claussen, C., Felix, R., James, A. E., Jr., Eds. *Contrast Agents in Magnetic Resonance Imaging*; Excerpta Medica: Princeton, NJ, 1986.
(5) Jezowska-Trzebiatowska, B.; Latos-Grazynski, L.; Kozlowski, H. *Inorg. Chim. Acta* **1977**, *21*, 145.
(6) Latos-Grazynski, L.; Jezowska-Trzebiatowska, B. *J. Coord. Chem.* **1980**, *10*, 159.
(7) Stezowski, J. J.; Hoard, J. L. *Isr. J. Chem.* **1984**, *24*, 323.
(8) Gries, H.; Miklautz, H. *Physiol. Chem. Phys. Med. NMR* **1984**, *16*, 105.
(9) Choppin, G. R.; Baisden, P. A.; Khan, S. A. *Inorg. Chem.* **1979**, *18*, 1330.
(10) Jenkins, B. G.; Lauffer, R. B. *J. Magn. Reson.* **1988**, *80*, 328.
(11) Desreux, J. F. *Inorg. Chem.* **1980**, *19*, 1319.
(12) Desreux, J. F.; Loncin, M. F. *Inorg. Chem.* **1986**, *25*, 69.
(13) Jeener, J.; Meier, B. H.; Bachmann, P.; Ernst, R. R. *J. Chem. Phys.* **1979**, *71*, 4546.
(14) States, D. J.; Haberkorn, R. A.; Ruben, D. J. *J. Magn. Reson.* **1982**, *48*, 286.
(15) Bodenhausen, G.; Vold, R. L.; Vold, R. R. *J. Magn. Reson.* **1980**, *37*, 93.
(16) Binsch, G. *Top. Stereochem.* **1968**, *3*, 97.

Table I. Kinetic Parameters for Conformational Dynamics of $Ln(DTPA)^{2-}$ [a]

Ln	$\Delta G^{\ddagger}_{298}$	$\Delta H^{\ddagger}$	$\Delta S^{\ddagger}$	k_{ex} 5 °C	k_{ex} 80 °C
Pr	56.5 ± 3.6	35.2 ± 2.0	−71.4 ± 5.8	265	8,430
Eu	55.4 ± 4.6	38.5 ± 2.4	−56.8 ± 7.0	360	16,000
Yb	49.4 ± 10.0	37.0 ± 5.0	−41.7 ± 16.2	4,300	163,000

[a] ΔG and ΔH values in kJ mol^{-1}; ΔS values in J mol^{-1} K^{-1}; k_{ex} values in s^{-1}. Exchange rates reported from interpolations of Arrhenius plots except for k_{ex} at 5 °C of Pr, which comes from EXSY data. Errors reported are ±2 standard deviations of fitted lines. Actual systematic errors may be considerably larger.

Table II. Observed and Calculated Isotropic Shifts for $Pr(DTPA)^{2-}$ [a]

label[b]	proton	δ_{obs}	δ_{calc}[c]	δ_{calc}[d]
r	H9B	−45.3	−43.2	−51.1
q	H5B	−43.1	−42.0	−47.4
p	H9A	−19.7	−21.5	−24.2
o	H6A	−18.7	−21.4	−24.0
n	H6B	−12.7	−12.7	−16.7
m	H7B	−8.8	−12.9	+0.8
l	H7A	−8.6	−10.9	−5.5
k	H5A	−7.5	−10.9	−17.2
j	H2B	−2.0	−8.0	+3.3
i	H10B	+4.0	+5.3	+1.3
h	H10A	+4.7	+1.2	−6.1
g	H13B	+10.1	+2.0	−5.3
f	H2A	+14.5	+10.0	+3.4
e	H3B	+19.6	+18.7	+7.3
d	H13A	+27.3	+19.8	+11.0
c	H11B	+28.6	+28.7	+16.1
b	H11A	+36.0	+36.2	+23.8
a	H3A	+36.9	+37.8	+22.0
	R		0.16	0.40

[a] Shifts are reported for the best fit to data calculated from proton coordinates of the crystal structure of NdDTPA.[7] Nd represents the origin of the coordinate system with the best-fit axes corresponding to the neodymium–water oxygen vector (see Figure 4) making an angle of 16.0° with the z axis and the projection of that vector in the x, y plane making an angle of 10.0° with the x axis (i.e. θ = 16.0°, ϕ = 10.0° for that vector). [b] Proton labels correspond to those in Figure 2a. [c] Calculated by using eq 5 in text, with $D_1 = -1250 \pm 125$ ppm Å^3 and $D_2 = -1250 \pm 300$ ppm Å^3. [d] Calculated by using eq 6 in text, with $D_1 = 1430 \pm 25$ ppm Å^3.

written by us utilizing a different iterative method (unpublished). Both methods minimize the agreement factor[18]

$$R = \left(\frac{\sum_i (\delta_{calc} - \delta_{obs})_i^2}{\sum_i (\delta_{obs})_i^2} \right)^{1/2} \quad (7)$$

Results and Discussion

Solution Dynamics of $Ln(DTPA)^{2-}$ Complexes. Shown in Figure 1 is the structure of DTPA with proton labels assigned from the crystal structure of NdDTPA.[7] The letters correspond to proton assignments reported later in Tables II and III.

One-dimensional ^1H NMR spectra as a function of temperature are shown in Figure 2 for $Pr(DTPA)^{2-}$, $Eu(DTPA)^{2-}$, and $Yb(DTPA)^{2-}$. At low temperatures 18 resonances are visible for $Pr(DTPA)^{2-}$, though the peaks marked l and m overlap considerably. At low temperatures 18 resonances can also be seen for $Eu(DTPA)^{2-}$, though one signal is buried beneath the HOD signal, and two at ca. −15 ppm overlap above 2 °C. For $Yb(DTPA)^{2-}$ two proton resonances, one acetate resonance and one ethylene resonance are obscured by solvent signals; however, none overlap. At high temperatures there are nine resonances for all three chelates, indicating that an exchange occurs between two symmetry related species.

Table III. Observed and Calculated Isotropic Shifts for $Yb(DTPA)^{2-}$ [a]

label[b]	proton	δ_{obs}	δ_{calc}[c]	δ_{calc}[d]
a	H9B	+142.9	+145.1	+127.6
b	H5B	+109.5	+102.7	+95.7
c	H6A	+84.0	+69.4	+79.7
d	H9A	+71.8	+78.8	+77.0
e	H6B	+66.2	+64.1	+76.6
f	H5A	+41.6	+44.0	+40.0
g	H7B	+25.1	+26.9	+47.3
h	H10A	+16.4	+17.7	+18.1
i	H7A	+1.0	+9.2	+41.2
j	H10B	−1.1	−1.9	+17.0
k	H3B	−8.1	−3.8	−19.3
l	H13B	−12.5	−8.6	−6.4
m	H2A	−35.9	−39.5	−39.7
n	H11A	−38.0	−49.4	−38.2
o	H13A	−50.7	−50.3	−40.1
p	H11B	−51.2	−52.5	−45.5
q	H3A	−53.5	−56.5	−62.7
r	H2B	−66.2	−64.1	−52.4
	R		0.094	0.232

[a] Shifts are reported for the best fit to data calculated from proton coordinates of the crystal structure of NdDTPA,[7] with Nd representing the origin of the coordinate system. The best-fit axes correspond to θ = 19.6°, ϕ = 57.2° for the neodymium–water oxygen vector. [b] Labels correspond to the chemical shift labels shown in Figure 2c. [c] Calculated by using eq 6 in text, with $D_1 = 3880 \pm 99$ ppm Å^3 and $D_2 = 3397 \pm 307$ ppm Å^3. [d] Calculated by using eq 5 in text, with $D_1 = 3957 \pm 229$ ppm Å^3.

In order to probe this exchange process in more detail, 2D EXSY spectra were utilized. This technique allows one to sample the entire exchange matrix in one experiment rather than perform a large number of saturation transfer experiments. The main problem with utilization of a technique involving incoherent magnetization transfer (such as EXSY) with paramagnetic molecules is shortened T_1's.[10] If $1/T_1$ is much greater than k_{ex}, then transverse magnetization will be destroyed by spin–lattice relaxation before appreciable cross-peak intensity can accumulate. By suitable adjustment of the mixing time (τ_m) this problem can be alleviated to a degree.

Shown in Figure 3 are EXSY spectra for $Pr(DTPA)^{2-}$, $Eu(DTPA)^{2-}$, and $Yb(DTPA)^{2-}$. A complete assignment of the exchanging partners is easily obtained by tracing the proton exchange connectivities. The spectra for $Eu(DTPA)^{2-}$ and $Pr(DTPA)^{2-}$ are extremely clean, whereas that of $Yb(DTPA)^{2-}$ contains considerably more noise. The relaxation times are much shorter in the case of $Yb(DTPA)^{2-}$, and this leads to a much more rapid decay of signal intensity.[10] Nonetheless, all the exchange pairs are easily resolved.

From the simple coalescence behavior (18 peaks to 9), we deduce that exchange is occurring between two enantiomers of each of the three complexes (i.e., racemization). The crystal structure of $Nd(DTPA)^{2-}$ indeed reveals a chiral complex that is viewed most straightforwardly as a monocapped square antiprism.[7] Three nitrogens and one oxygen from a terminal acetate form the bottom square face and the four remaining acetate oxygens form the top face; the 9-coordinate complex is capped with a water molecule (Figure 4). The major feature of the exchange process essentially involves the shuffling of coordinated acetates as shown in Figure 4: the lone terminal acetate in the bottom face is displaced to the top face while another terminal acetate takes its place. The positions of the other acetates (and possibly the water molecule) are also altered in this process. In addition, the ethylenes flip between staggered conformations. (Evidence for solution structures similar to the Nd(III) crystal structure is presented below.)

Exchange rates for this racemization process can be calculated from coalescence temperatures. Since there are so many protons, we can follow the 1D spectra as a function of temperature and obtain a number of different coalescence temperatures. In addition, following the coalescence at two (or more) frequencies

(17) Sherry, A. D.; Tehrani, J. *J. Biol. Chem.* **1983**, *258*, 8663.
(18) Hamilton, W. R. *Acta Crystallogr.* **1965**, *18*, 502. Willcott, M. R., III; Lenkinski, R. E.; Davis, R. E. *J. Am. Chem. Soc.* **1972**, *94*, 1742.

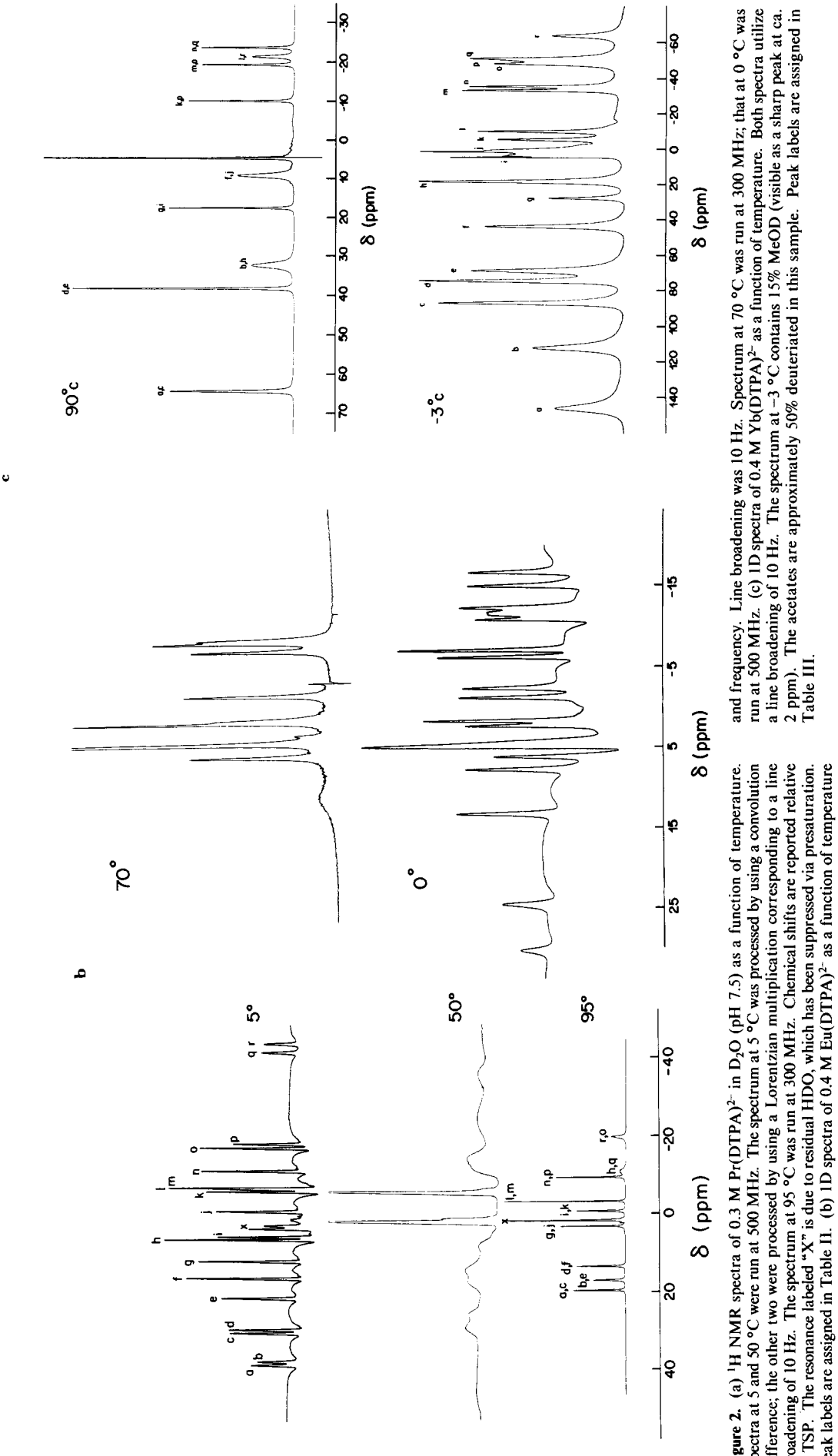

Figure 2. (a) ^{1}H NMR spectra of 0.3 M Pr(DTPA)$^{2-}$ in D_2O (pH 7.5) as a function of temperature. Spectra at 5 and 50 °C were run at 500 MHz. The spectrum at 5 °C was processed by using a convolution difference; the other two were processed by using a Lorentzian muliplication corresponding to a line broadening of 10 Hz. The spectrum at 95 °C was run at 300 MHz. Chemical shifts are reported relative to TSP. The resonance labeled "X" is due to residual HDO, which has been suppressed via presaturation. Peak labels are assigned in Table II. (b) 1D spectra of 0.4 M Eu(DTPA)$^{2-}$ as a function of temperature and frequency. Line broadening was 10 Hz. Spectrum at 70 °C was run at 300 MHz; that at 0 °C was run at 500 MHz. (c) 1D spectra of 0.4 M Yb(DTPA)$^{2-}$ as a function of temperature. Both spectra utilize a line broadening of 10 Hz. The spectrum at −3 °C contains 15% MeOD (visible as a sharp peak at ca. 2 ppm). The acetates are approximately 50% deuteriated in this sample. Peak labels are assigned in Table III.

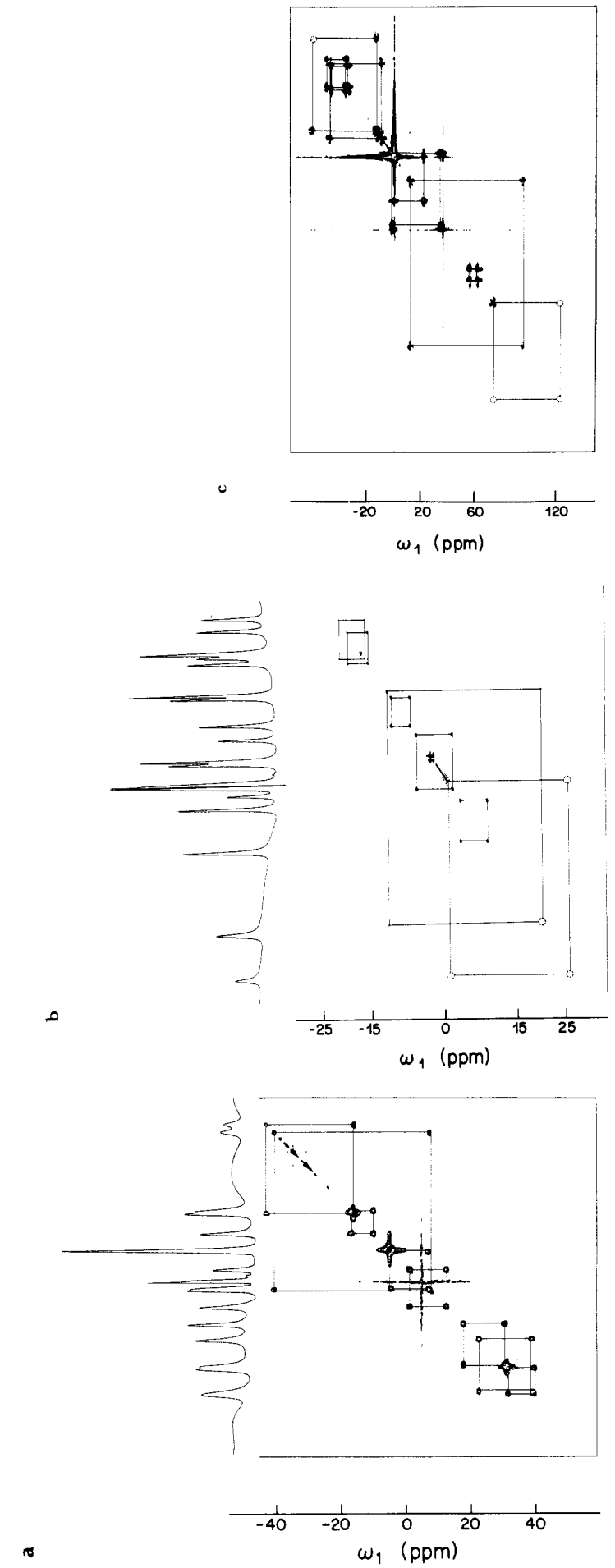

Figure 3. (a) Contour plot of the EXSY spectrum of 0.3 M $Pr(DTPA)^{2-}$ at 500 MHz and 25 °C. Mixing time was 15 ms. Final data matrix was 1K × 1K without zero filling. The data were processed by using a Lorentzian multiplication corresponding to 10 Hz line broadening in F_2 and a convolution difference in F_1. The spectrum has been symmetrized about the diagonal. (b) Similar EXSY spectrum for $Eu(DTPA)^{2-}$ at 3 °C, processed in F_1 and F_2 by using the same apodizations as in part a. Mixing time was 10 ms. (c) Similar EXSY spectrum for $Yb(DTPA)^{2-}$ at 0.1 °C, processed in F_1 and F_2 by using the same apodizations as in part a. Mixing time was 1 ms. This sample was undeuteriated. Dotted circles for both $Eu(DTPA)^{2-}$ and $Yb(DTPA)^{2-}$ represent cross and diagonal peaks not seen at this contour level. This is for clarity only; these peaks are easily seen at lower contour levels.

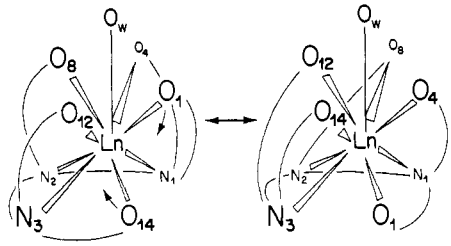

Figure 4. Schematic for the conformational rearrangement taking place in $Ln(DTPA)^{2-}$ showing the movement of coordinated acetates. Labels correspond to those in ref 7.

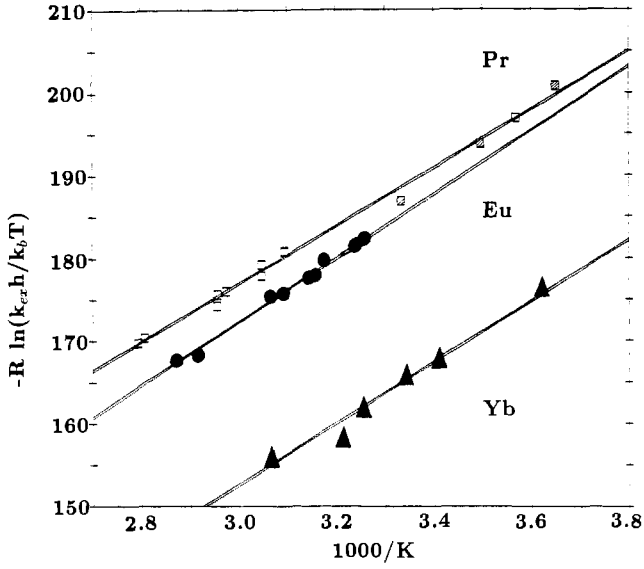

Figure 5. Eyring plot for the kinetics of racemization in $Ln(DTPA)^{2-}$. Data for Pr(III) and Eu(III) were obtained at 300 and 500 MHz; those for Yb(III) were obtained at 300 MHz. The three crosshatched squares represent data from EXSY spectra as described in the Experimental Section.

increases the number of data points and the temperature range. Traditionally, activation parameters derived from coalescence temperatures are considered unreliable (cf. ref 16) largely because such a small temperature range is covered. Our results presented in Figure 5 and Table I derive from data collected over a temperature range of ~0–85 °C. Utilization of 2D EXSY helps one to overcome this limitation for molecules with large numbers of protons. Exchange rates were calculated by using the well-known expression

$$k_{ex} = \pi\delta\nu/\sqrt{2} \qquad (8)$$

where $\delta\nu$ is the frequency separation (in Hz) between the two exchange partners at the coalescence temperature. The chemical shift differences were corrected empirically for the temperature dependence of the individual resonances. In addition, three exchange rates were determined for $Pr(DTPA)^{2-}$ from EXSY spectra by using the method outlined in the experimental section.

The exchange rates determined are presented in Figure 5 in the form of an Eyring plot (with the transmission coefficient set equal to 1); the activation parameters are shown in Table I. From Figure 5 it is apparent that the points determined from the EXSY data (shown as crosshatched squares) are in general agreement with those determined from coalescence temperatures, thus lending credence to the activation parameters.

From these data it is apparent that the activation enthalpies are similar for all three lanthanide complexes, indicating that similar barriers to interconversion exist and that the same process most likely occurs for each complex. The activation entropies, on the other hand, appear to vary significantly between the three complexes, leading to the order of exchange rates observed: $Pr(DTPA)^{2-} < Eu(DTPA)^{2-} < Yb(DTPA)^{2-}$. While we cannot rule out some degree of error in these values due to the possibility of relatively large systematic errors (cf ref 19) (including the necessity of correcting for the temperature dependence of the paramagnetic shifts), we believe that the entropy changes are important in determining the relative exchange rates.

It is useful to compare the structure and dynamics of these $Ln(DTPA)^{2-}$ complexes to the analogous macrocyclic DOTA complexes studied by Desreux and co-workers.[11] Like the $Nd(DTPA)^{2-}$ complex, the crystal structure of $Eu(DOTA)^{2-}$ reveals that the complex can be idealized as a monocapped square antiprism: the 12-membered nitrogen macrocycle forms the bottom square face, the acetates form the top face, and a water molecule completes the coordination sphere.[20] The intramolecular dynamics of the $Ln(DOTA)^-$ complexes originate from ethylene "flip-flops" where staggered ethylenes along the 12-membered ring flip to their enantiomeric conformation via an eclipsed transition state; a high activation enthalpy of approximately 60 kJ/mol was determined for $La(DOTA)^-$. It is not clear how much of this energy barrier is due solely to the macrocyclic nature of the ligand and how much is due to the transition-state eclipsed conformation itself. This energy barrier is much higher than the $\Delta H^{\ddagger}$ estimated for the three $Ln(DTPA)^{2-}$ complexes in the present work (35–40 kJ/mol). This is consistent with the fact that $Ln(DOTA)^-$ has four ethylene groups to only two for $Ln(DTPA)^{2-}$, thus creating a higher "eclipsed" ethylene transition barrier. The fact that the racemization process in $Ln(DOTA)^-$ requires only slight movements of the acetate groups whereas the racemization in $Ln(DTPA)^{2-}$ requires large movements of coordinated acetates (see Figure 4) may also be important in determining the relative activation parameters.

The exchange process in $Ln(DTPA)^{2-}$ is more similar to that of $Ln(DOTA)^-$ than $Ln(TETA)^-$. In $Ln(TETA)^-$ differing exchange processes occur for the Pr(III) complex when compared to the Yb(III) and Eu(III) complexes.[12] The Pr(III) complex is in slow exchange by NMR criteria only at −55 °C. This presumably occurs as a result of the larger size of Pr(III). Because of the more flexible nature of DTPA compared to DOTA, one would assume differing exchange processes would also be possible as a function of ion size in the case of $Ln(DTPA)^{2-}$. Our data clearly show that this does not occur.

In comparison of the dynamics of these complexes, the factors that can give rise to "rigidity" (or slow-exchange NMR behavior) in lanthanide complexes become evident. It is especially important to note that, as shown for the DTPA complexes, a macrocyclic ligand system is not required to slow down the conformational exchange process: the exchange rates for $Pr(DTPA)^{2-}$ are only an order of magnitude faster than $La(DOTA)^-$ and they are much slower than that commonly observed for lanthanide complexes.[2] We believe that relatively "rigid" behavior in a lanthanide chelate is likely to exist where a highly multidentate ligand is capable of realizing its full denticity.

COSY Spectra. The use of COSY spectra enables one to determine interproton scalar J couplings, which can be invaluable in aiding the assignment of specific resonances. However, similar limitations that apply to the detection of cross peaks with respect to T_1 in EXSY spectra apply to the detection of cross peaks in COSY spectra with respect to T_2.[10] Short T_2 values cause rapid decay of phase coherence, which attenuates cross-peak intensity before it has a chance to accumulate. In the case of paramagnetic lanthanide(III) complexes with relatively short metal–proton distances at high fields and low temperatures, the Curie spin mechanism will be a major contribution to T_2.[10,21,22] This makes detection of cross-peak intensity quite difficult. (A diagnostic for dominant Curie contributions is the observation that $T_2 \ll T_1$ for chelates where $\omega_0\tau_r < 1$.) Due to its inverse square dependence on temperature and quadratic dependence on magnetic field, one way to circumvent the Curie effect is to run spectra at high

(19) Newman, K. E.; Meyer, F. K.; Merbach, A. E. *J. Am. Chem. Soc.* **1979**, *101*, 1470.
(20) Spirlet, M. R.; Rebizant, J.; Desreux, J. F.; Loncin, M. F. *Inorg. Chem.* **1984**, *23*, 359.
(21) Guéron, M. *J. Magn. Reson.* **1975**, *19*, 58.
(22) Burns, P. D.; LaMar, G. N. *J. Magn. Reson.* **1982**, *46*, 61.

temperatures and lower fields. The high-temperature requirement prevented the study of COSY spectra in the slow-exchange limit; thus, the results presented below are from exchange-averaged resonances.

In order to ascertain that coupling is indeed visible in the rapid-exchange limit, COSY spectra were run on diamagnetic $La(DTPA)^{2-}$ complexes. Shown in Figure 6a is a COSY spectrum of $La(DTPA)^{2-}$ at 70 °C. At this temperature, the molecule is well into the fast-exchange limit and the spectrum is readily interpreted (interestingly, interpretation of the corresponding paramagnetic spectrum is easier due to the lack of resolved scalar coupling). The rapid exchange averages the J coupling of the ethylenes (all protons < 3.2 ppm) such that two proton resonances exhibit only one averaged cross peak to their geminal (on the same carbon) partners. These geminal couplings average about 16 Hz for both the acetates and ethylenes. The acetate COSY pattern is a classic AX-type COSY pattern with couplings between the geminal partners (i.e. coupling between, e.g., H2A and H13A at one frequency and H2B and H13B at another frequency).

Thus, similar couplings should be evident in COSY spectra of the paramagnetic analogues, provided the T_2's are long enough to allow cross-peak intensity to accumulate. In practice, this means that T_2's should generally be $\geq 1/5J$ s.[23,24] At 90 °C and 250 MHz, COSY spectra of the paramagnetic chelates show that detection of cross peaks is possible, though difficult.

Shown in Figure 6b,c are COSY spectra of $Yb(DTPA)^{2-}$ and $Pr(DTPA)^{2-}$ at high temperatures. The expected number of cross peaks is four (two ethylenes and two acetates; the central acetate has coalesced to a single peak), though not all of these are visible. In the case of $Pr(DTPA)^{2-}$ the two acetate cross peaks are visible whereas the two ethylenic cross peaks are not. This fact indicates that exchange line broadening rather than the Curie effect is the dominant contributor to T_2 at these temperatures.[10] In the case of $Yb(DTPA)^{2-}$, cross peaks are visible for one sharp ethylene pair and one acetate pair. This, by elimination, assigns the other pair of ethylenes and the two most downfield acetates, since the peak at ca. 15 ppm represents the central acetates.

Pseudocontact Shift Calculations. Through the use of the EXSY and COSY experiments, we now have a set of constraints that allow us to utilize chemical shift calculations (eq 5 and 6) to completely assign the protons. For instance, in the case of $Pr(DTPA)^{2-}$, the protons a,c and b,e represent exchange partners on two different terminal acetates (by EXSY). The COSY spectrum indicates that a,e and b,c are partners on the same carbons (i.e. a and e are on one particular acetate, and b and c are on another). Similar reasoning can be followed for the other protons. We note that the EXSY and COSY information in this case is complementary, and certainly the latter data would be impossible to obtain from a 1D experiment.

The results of the dipolar shift calculations for $Pr(DTPA)^{2-}$ and $Yb(DTPA)^{2-}$ are presented in Tables II and III, respectively. These results represent the "best" fits in the sense that they represent the smallest R factors,[18] after calculation with eq 5 and 6, that are also consistent with the NMR data. In both cases the z susceptibility axis is close to being parallel with the metal–water oxygen vector (see Figure 4). It is important to note that other fits exist with reasonably small R factors (<0.20). During the fitting procedure the only way to discriminate between possible solutions is through the use of both the COSY and the EXSY data. For instance, merely switching the assignments of the ethylene protons H9A and H6A in Table III would result in lowering the R factor from 0.094 to 0.073. Use of the R factor ratio test[18] indicates that rejection of the 0.094 fit would be wrong only ≈1% of the time. The fit with R = 0.073, is, however, inconsistent with the EXSY exchange data (i.e. it has two protons on the same carbon, H9A and H9B, exchanging with one another). Without the extremely detailed constraints of the EXSY and COSY data, assignments for all the shifts would have been impossible to attain short of chemically labeling every other proton. While we believe that these fits represent the best solutions consistent with the rather severe constraints of the EXSY and COSY data, fortuitous agreement cannot be completely ruled out.

The sources of the discrepancy between the observed and calculated shifts for $Pr(DTPA)^{2-}$ are likely to arise from appreciable, though not dominant, Fermi contact contributions to the chemical shifts. Since Pr(III) is closer in size to Nd(III) (the metal used in the crystal structure) than Yb(III), it is likely that these differences do not arise from discrepancies between the crystal structure of $Nd(DTPA)^{2-}$ and the solution structure of $Pr(DTPA)^{2-}$ since $Yb(DTPA)^{2-}$ gave quite a good fit. It is well-known that Yb(III) generally produces the smallest contact contributions to chemical shifts of all the paramagnetic lanthanides.[26-28]

Even though the fits for $Pr(DTPA)^{2-}$ are not completely satisfactory, they do provide very good qualitative agreement in the sense of correctly reproducing the signs of the shifts and they provide good qualitative agreement for the larger shifts. These large shifts (i.e. H9a,b H5b, H3a, H11a) are most likely correct, as every model consistent with the EXSY and COSY data and with an R factor less than 0.3 converged to the same assignments. In addition, both computational methods utilized reached these same assignments, thus supporting their veracity. The other assignments, though not as ironclad as the large shifts, are most likely correct, as the EXSY and COSY data place severe constraints upon the number of possible combinations.

Coordination of the Central Acetate. On a final note we address the problem of coordination of the central acetate. Various investigators have proposed that the oxygen of the central acetate in $Ln(DTPA)^{2-}$ complexes is not coordinated in solution. However, most of the evidence is indirect and incomplete. First, the results of ref 9 were interpreted as being due to noncoordination of the central acetate. This conclusion was based on the fact that one of the acetates in the room-temperature spectrum of $La(DTPA)^{2-}$ was a singlet. Aside from the fact that this spectrum represented the fast-exchange limit, there was no reason to assign this singlet to the central acetate; it could just as well represent a terminal acetate. In the context of our results it can be assigned as being the central acetate; however, the fact that it appears as a singlet is due to exchange averaging, not necessarily uncoordination. Further evidence comes from thermodynamic results of complexation of DTPA with lanthanides where enthalpies were consistent with coordination of three nitrogens and entropies were interpreted to be consistent with coordination of only four acetates.[29] Other indirect evidence rises from an empirical fit to the ^{139}La NMR chemical shift in various polyamino polycarboxylate ligands, which was interpreted in the case of $La(DTPA)^{2-}$ as being consistent with only four coordinated oxygens.[30]

Our NMR studies of the three paramagnetic DTPA complexes as well as $La(DTPA)^{2-}$ provide *no* evidence that the central acetate is not coordinated or has a shorter M–O lifetime than the terminal acetates. An uncoordinated, freely rotating acetate methylene would (barring large anisotropic contact shifts) give rise to a two-proton singlet. Since all 18 individual protons of the three paramagnetic complexes were observed at low temperatures and the coalescence behavior was consistent with only a single process,

(23) Bax, A.; Freeman, R. *J. Magn. Reson.* **1981**, *44*, 542.
(24) One way to relax this limitation would be to acquire *hetero*nuclear ^1H–^{13}C COSY spectra. Since one-bond ^1H–^{13}C couplings are on the order of 100 Hz, cross peaks could be detected in molecules where T_2 values are a factor of about 5 less than those in the comparable ^1H–^1H case. Indeed, heteronuclear COSY measurements have been obtained in the case of a low-spin iron met-cyano complex of myoglobin,[25] though the T_2 values in that complex are considerably longer than those here.
(25) Yamamoto, Y. *FEBS Letters* **1987**, *222*, 115.
(26) Horrocks, W. D. In *NMR of Paramagnetic Molecules*; LaMar, G. N., Horrocks, W. D., Holm, R. H., Eds.; Academic Press: New York, 1973; Chapter 12.
(27) Reilley, C. N.; Good, B. W.; Allendoefer, R. D. *Anal. Chem.* **1976**, *48*, 1446.
(28) Shelling, J. G.; Bjornson, M. E.; Hodges, R. S.; Taneja, A. K.; Sykes, B. D. *J. Magn. Reson.* **1984**, *57*, 99.
(29) Choppin, G. R.; Goedken, M. P.; Gritmon, T. F. *J. Inorg. Nucl. Chem.* **1977**, *39*, 2025.
(30) Geraldes, C. F. G. C.; Sherry, A. D. *J. Magn. Reson.* **1986**, *66*, 274.

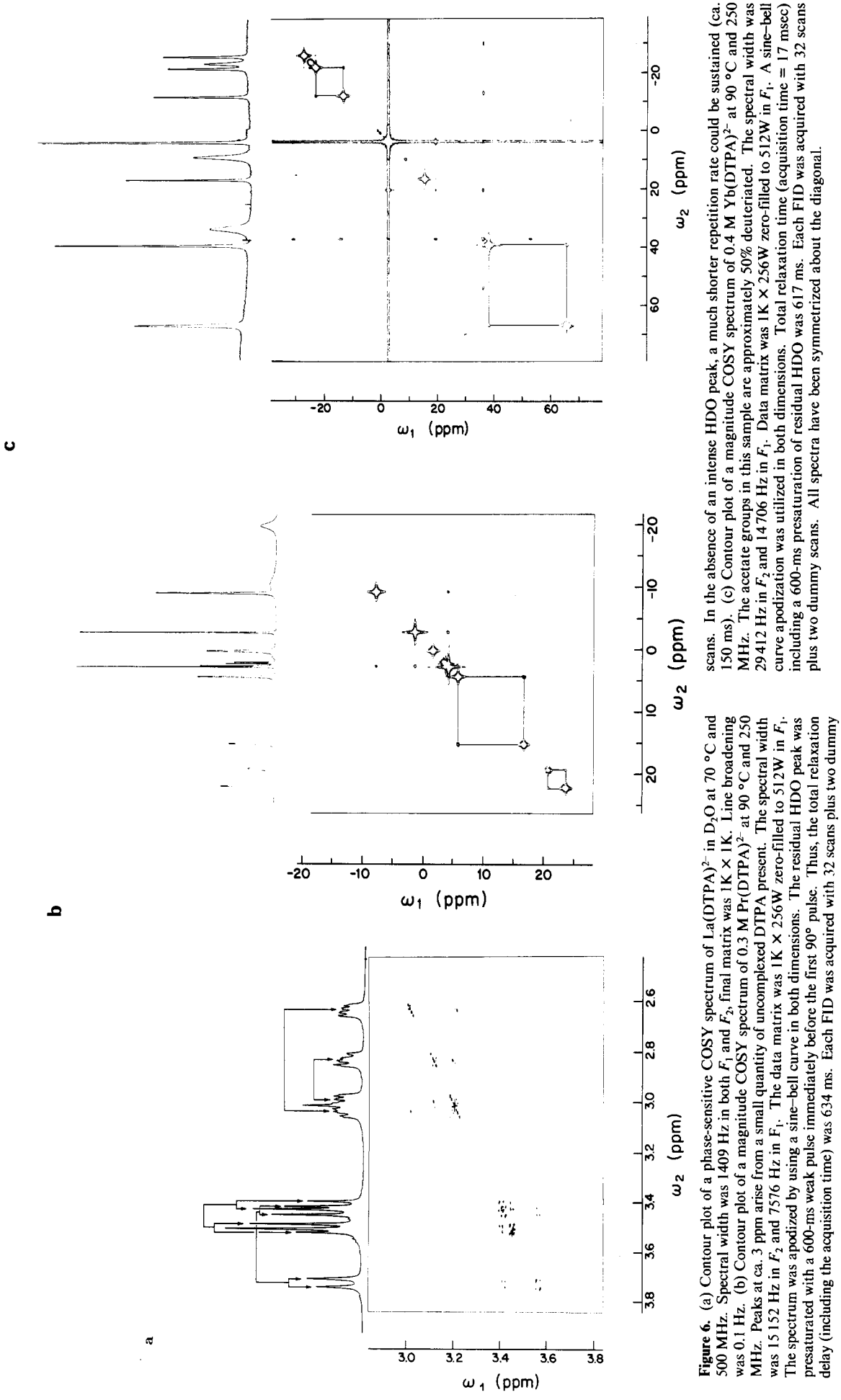

Figure 6. (a) Contour plot of a phase-sensitive COSY spectrum of $La(DTPA)^{2-}$ in D_2O at 70 °C and 500 MHz. Spectral width was 1409 Hz in both F_1 and F_2, final matrix was 1K × 1K. Line broadening was 0.1 Hz. (b) Contour plot of a magnitude COSY spectrum of 0.3 M $Pr(DTPA)^{2-}$ at 90 °C and 250 MHz. Peaks at ca. 3 ppm arise from a small quantity of uncomplexed DTPA present. The spectral width was 15152 Hz in F_2 and 7576 Hz in F_1. The data matrix was 1K × 256W zero-filled to 512W in F_1. The spectrum was apodized by using a sine-bell curve in both dimensions. The residual HDO peak was presaturated with a 600-ms weak pulse immediately before the first 90° pulse. Thus, the total relaxation delay (including the acquisition time) was 634 ms. Each FID was acquired with 32 scans plus two dummy scans. In the absence of an intense HDO peak, a much shorter repetition rate could be sustained (ca. 150 ms). (c) Contour plot of a magnitude COSY spectrum of 0.4 M $Yb(DTPA)^{2-}$ at 90 °C and 250 MHz. The acetate groups in this sample are approximately 50% deuteriated. The spectral width was 29412 Hz in F_2 and 14706 Hz in F_1. Data matrix was 1K × 256W zero-filled to 512W in F_1. A sine-bell curve apodization was utilized in both dimensions. Total relaxation time (acquisition time = 17 msec) including a 600-ms presaturation of residual HDO was 617 ms. Each FID was acquired with 32 scans plus two dummy scans. All spectra have been symmetrized about the diagonal.

it is doubtful that the central acetate is uncoordinated for any significant period of time. In our work, partial deuteriation allowed the assignment of the central acetate resonances. While the two resonances stemming from this group were quite close in chemical shift for the Pr(III) complex, they differ by 24 ppm in the Yb(III) complex.

These results are consistent with the solid-state structures of both Nd- and $Gd(DTPA)^{2-}$ as well as certain solution-state properties. From a correlation of luminescence wavelengths with total charge donated from a given ligand, Albin and Horrocks estimated the charge on $Eu(DTPA)^{2-}$ to be -5.3, implying full coordination by all five acetates.[31] Additionally, water ^1H relaxation data for $Gd(DTPA)^{2-}$[32] and luminescence studies on the Eu(III) complex[33] are consistent with a single coordinated water molecule as found in the crystal structures mentioned above; this supports the coordination of the central acetate since its displacement should open up an additional coordination site for water.

Conclusions

In conclusion, we have demonstrated that 2D NMR methods can play a vital role in assignment of the solution structural properties of lanthanide chelates. In solution, $Ln(DTPA)^{2-}$ chelates undergo a dynamic exchange between two enantiomers. This isomerization involves exchanges of coordinated terminal acetates between the top and bottom faces of the square-antiprismatic complex. The rates of this exchange process are similar to those seen in the macrocyclic chelates $Ln(DOTA)^-$ and $Ln(TETA)^-$. Calculation of the chemical shifts for the $Ln(DTPA)^{2-}$ chelate protons reveals that the shifts are predominantly dipolar in origin. These calculations clearly demonstrate that assignment of resonances (and hence geometry) merely by obtaining good fits between observed and calculated numbers is quite dangerous. The use of COSY and EXSY data provides invaluable evidence that can be used to constrain the fits and provide clear-cut answers to which fits among the number of possible fits are wrong. The solution structure of the chelates (including coordination of the central acetate) agrees well with the crystal structures determined for $Gd(DTPA)^{2-}$ and $Nd(DTPA)^{2-}$.

Acknowledgment. This work was supported by PHS Grant GM37777, awarded by the National Institute of General Medical Sciences. NMR experiments at 500 MHz were run at the Francis Bitter National Magnet Laboratory, MIT, supported by Grant RR00995 from the Division of Research Resources of the NIH and Contract C-670 from the National Science Foundation. We thank Dr. A. Dean Sherry for providing a copy of his computer program for performing chemical shift calculations.

Registry No. $[Pr(DTPA)(H_2O)]^{2-}$, 76147-47-2; $[Eu(DTPA)(H_2O)]^{2-}$, 76166-31-9; $[Yb(DTPA)(H_2O)]^{2-}$, 76147-40-5.

(31) Albin, M.; Horrocks, W. D. *Inorg. Chem.* **1985**, *24*, 895.
(32) Koenig, S. H.; Brown, R. D., III. In *Magnetic Resonance Annual*; Kressel, H. Y., Ed.; Raven Press: New York, 1987.
(33) Bryden, C. C.; Reilley, C. N. *Anal. Chem.* **1982**, *54*, 610.

Contribution from the Department of Chemistry, Emory University, Atlanta, Georgia 30322, and Dipartimento di Scienze Chimiche, Università di Trieste, 34127 Trieste, Italy

Organocobalt B_{12} Models Bearing Axial Substituents on a Costa-Type Equatorial Ligand: Structural, Rate, and Spectroscopic Consequences

Paulos G. Yohannes,[†] Nevenka Bresciani-Pahor,[‡] Lucio Randaccio,*[,‡] Ennio Zangrando,[‡] and Luigi G. Marzilli*[,†]

Received March 25, 1988

Several new organocobalt complexes of the type $[LCo((DO)(DOH)Me_2pn)CH_3]X$ were synthesized from $Co((DO)(DOH)Me_2pn)Br_2$, where L = neutral N- or P-donor ligand and $(DO)(DOH)Me_2pn$ = $N^2,N^{2'}$-2,2-dimethylpropanediylbis(2,3-butanedione 2-imine 3-oxime). These were characterized by ^1H NMR spectroscopy and, in a few cases, by ^{13}C NMR spectroscopy. The rates of L ligand dissociation were found to be greater than those of the analogous Costa model complexes, where the equatorial ligand, (DO)(DOH)pn, has a propylene bridge in place of the 2,2-dimethylpropylene bridge, or the analogous cobaloxime complexes. The three-dimensional structures of two of these new complexes, $[LCo((DO)(DOH)Me_2pn)CH_3]PF_6$, in which L = pyridine (py) (I) and L = 1,5,6-trimethylbenzimidazole (Me_3Bzm) (II), were determined. Crystallographic details are as follows: I, $C_{19}H_{31}CoF_6N_5O_2P$, $P2_12_12_1$, a = 12.718 (3) Å, b = 12.861 (2) Å, c = 15.437 (3) Å, D(calcd) = 1.49 g cm^{-3}, Z = 4, R = 0.048 for 2923 independent reflections; II, $C_{24}H_{38}CoF_6N_6O_2P\cdot{}^1/_2H_2O$, *Pbca*, a = 14.103 (3) Å, b = 17.415 (2) Å, c = 24.555 (3) Å, D(calcd) = 1.44 g cm^{-3}, Z = 8, R = 0.048 for 3208 independent reflections. The structures of these two derivatives are similar to those of the analogous (DO)(DOH)pn compounds, except that the planar py and Me_3Bzm ligands lean away from the 2,2-dimethylpropylene group. The plane of L makes an angle of ~80° with the plane of the equatorial ligand. This result is attributed to steric effects. These steric effects are believed to account for the increased rate of L dissociation compared to that in the parent model system. In addition, ^1H and ^{13}C chemical shifts of L are upfield in the $(DO)(DOH)Me_2pn$ compounds. This observation is attributed to equatorial ligand anisotropy and strongly indicates that ^1H and ^{13}C NMR shifts of L in organocobalt models reflect ligand anisotropy, as well as Co anisotropy.

Introduction

With the growing recognition that the role of the Co center in coenzyme B_{12} (5′-deoxyadenosylcobalamin) dependent enzymic processes is probably limited to providing a facile source of 5′-deoxyadenosyl radical via Co-C bond homolysis,[1,2] interest has refocused on the factors promoting cleavage of this bond.[1-4] Conformational changes in the coenzyme that accompany substrate-induced conformational changes in the B_{12} holoenzymes are almost certainly responsible for promoting cleavage.[1-4] For some time, we have been interested in elucidating changes in conformation of organocobalt species that promote cleavage.[3-5]

[†] Emory University.
[‡] Università di Trieste.

(1) Halpern, J. *Science (Washington, D.C.)* **1985**, *227*, 869. Halpern, J.; Kim, S. H.; Leung, T. W. *J. Am. Chem. Soc.* **1984**, *106*, 8317. Halpern, J. *Pure Appl. Chem.* **1983**, *55*, 1059. Halpern, J. In B_{12}; Dolphin, D., Ed.; Wiley: New York, 1982; Vol. 1, p 501. Ng, F. T.; Rempel, G. L.; Halpern, J. *Inorg. Chim. Acta* **1983**, *77*, L65. Halpern, J. *Ann. N.Y. Acad. Sci. (U.S.A.)* **1974**, *239*, 2.
(2) Finke, R. J.; Schiraldi, D. A.; Mayer, B. J. *Coord. Chem. Rev.* **1984**, *31*, 105. Finke, R. G.; Hay, B. P. *Inorg. Chem.* **1984**, *23*, 3041. Hay, B. P.; Finke, R. J. *J. Am. Chem. Soc.* **1986**, *108*, 4820. Hay, B. P.; Finke, R. G. *J. Am. Chem. Soc.* **1987**, *109*, 8012.
(3) Bresciani-Pahor, N.; Forcolin, M.; Marzilli, L. G.; Randaccio, L.; Summers, M. F.; Toscano, P. J. *Coord. Chem. Rev.* **1985**, *63*, 1.

0020-1669/88/1327-4738$01.50/0